WILEY | Hindawi

Research Article

Study on Stress Disturbed Mechanism and Supporting Method of Weakly Cemented Roadway near Chambers

Wei Zhang ⓘ

School of Architecture and Engineering, Liaocheng University, Liaocheng 252000, China

Correspondence should be addressed to Wei Zhang; zhangw@lcu.edu.cn

After excavation of the weakly cemented roadway adjacent to the chambers, deformation characteristics such as roof subsidence, roadway extrusion, and floor heave appear, showing the characteristics of large deformation of surrounding rock, long deformation duration, and serious damage, which are not conducive to guaranteeing safety mining. Based on the technical means of the rock mechanical property test, mineral composition analysis, in situ stress test, and surrounding rock deformation monitoring of 2# coal roadway in Hongqingliang coal mine, a numerical simulation study on the influence of surrounding rock stress on adjacent chamber groups was carried out. The physical and mechanical properties of the weakly cemented rock were obtained, the stress distribution law of the 2# coal roadway was mastered, the deformation characteristics of the surrounding rock of the weakly cemented roadway were obtained, and the deformation and failure mechanism of the weakly cemented roadway adjacent to the chambers were revealed. The relationship between the regional stress increment of the chambers and the failure range of the surrounding rock of the roadway is revealed, establishing a mechanical model of allowable deformation + stress release + controlled form with U-shaped steel as the main structure. The roadway support countermeasures were given and applied in engineering practice.

1. Introduction

As the shallow coal resources in the central and eastern parts of China tend to be exhausted, the mining of mines gradually extends to the deep parts and develops into the western mining areas with rich coal resources such as Inner Mongolia. Weakly cemented soft rocks are widely distributed in the Jurassic and Cretaceous strata in the western mining area. Weakly cemented soft rock has poor cementation, low strength, easy weathering, and disintegration in case of cementation and belongs to a special kind of soft rock [1–3]. After the weakly cemented roadway is excavated, the surrounding rock is severely deformed and damaged, and it is difficult to effectively maintain the stability and safety of the surrounding rock of the roadway by the combined support of conventional bolts and bolts and the method of bolt mesh and shotcrete support [4]. The main performance is that the anchorage of active supporting structures such as anchor rods and anchor cables is poor, and the anchor rods and

anchor cables easily lose their anchoring force. The applied preload is small, and the supporting effect is poor. Passive support structures such as the concrete shotcrete layer bear a large pressure on the surrounding rock, and the structures are deformed and damaged due to local distortion [5].

The roof subsidence, floor heave, and two sides contraction of weakly cemented roadway are the results of large deformation of surrounding rock. On the basis of analyzing the large deformation mechanism of soft rock, He [6] constructed a mechanical analysis and design system for large deformation of soft rock engineering. Zhou et al. [7] analyzed the compound failure mechanism of molecular expansion + rock mass structural plane dislocation + excavation disturbance of surrounding rock of the soft rock roadway in accordance with the nonlinear large deformation failure phenomenon of Mesozoic composite soft rock in the Shajihai mining area, and Shang et al. [8] analyzed the deformation and failure characteristics and types of surrounding rock of soft rock roadway and

discussed the deformation and failure mechanism of the soft rock surrounding rock. Chen et al. [9] used the thickness of the surrounding rock loose zone to quantitatively determine the characteristics of surrounding rock in soft rock engineering and analyzed its nonlinear deformation and failure mechanism. Daniel et al. [10] considered the influence of roadway section shape, surrounding rock strength characteristics, and roadway group disturbance and revealed the large deformation mechanism of a broken soft rock roadway. On the basis of analyzing the deformation and failure characteristics of soft rock roadway, Meng et al. [11] carried out research on the evolution law, monitoring analysis, and support optimization design of surrounding rock of roadway in weak cementation stratum and revealed the deformation and failure mechanism of surrounding rock of a deep soft rock roadway. Zhang et al. [12] discussed the failure characteristics and deformation failure mechanism of the Jurassic Cretaceous argillaceous weakly cemented roadway and proposed that the surrounding rock softening in water, strong expansibility, and unreasonable support form are the main factors causing its deformation and failure. Chen et al. [13] analyzed the deformation and failure process of argillized weak cemented soft rock rectangular roadway, compared the simulation results with the field monitoring results, and gave suggestions on the selection of roadway section, shape, and support.

The surrounding rock reinforcement control technology adjacent to the chamber is the key to ensure the safe utilization of weak cementation roadway and has become a research hotspot in the engineering field. Kang et al. [14] obtained countermeasures to improve the stability of surrounding rock of the cavern group according to the stress distribution characteristics of surrounding rock of cavern group under soft rock conditions. Wang et al. [15] put forward a new concept of cracking inhibition for stability optimization of large caverns under soft rock conditions. Sun et al. [16] found the zonal fracture phenomenon and fracture distribution characteristics of weakly cemented surrounding rock through on-site monitoring, providing a basis for its reinforcement and support. Yang et al. [17] obtained the failure characteristics and control measures of the surrounding rock of the cavern group through the field test and numerical simulation method. He et al. [18] put forward the asymmetric control technology of "weak structure" to solve the problem of asymmetric deformation of soft rock caverns, laying a foundation for exploring the control theory and technology of caverns.

Although some scholars have studied the deformation and failure characteristics and mechanism of the soft rock roadway, the deformation and failure characteristics of the weak cemented soft rock roadway adjacent to the chamber group are different from those of ordinary soft rock roadway, which is still in the exploration stage. Based on the fracture development characteristics obtained by means of borehole televiwering, it was found that the sidewalls needed to be reinforced, and a support scheme "bolt cable- + bolt + supporting plate + metal mesh" was proposed for the roadway [19, 20]. A differentiated support scheme with

the core of "upgrading the support level and optimizing the support of large deformation area" was proposed to control the large deformations in the roadway area by strengthening the bearing capacity of the surrounding rock itself [21, 22]. In this study, the weak cemented soft rock in Hongqingliang mine is taken as the research object. Based on the surrounding rock deformation and support structure stress monitoring analysis and numerical simulation technology research, the deformation and failure characteristics of the weak cemented soft rock roadway adjacent to the chambers are analyzed, and its deformation and failure mechanism is studied, which lays a foundation for the control theory and technology research of an argillaceous weak cemented soft rock roadway.

2. Ground Pressure Behavior Characteristics of Weak Cemented Roadway

Hongqingliang mine is located in Inner Mongolia, with a design production capacity of 6 Mt/a and vertical shaft development. Among them, the section shape of 2# coal roadway is a straight wall semicircle arch, and the buried depth of the roadway is about 420 m. The combined support mode of "bolt mesh spraying + bolt + anchor cable" is adopted. The surrounding rock of 2# coal roadway is mainly a weak rock stratum such as weakly cemented mudstone and sandy mudstone, with poor integrity and low bearing capacity. There are 8 roadways and 15 groups of chambers of 3-coal within 30 m below 2# coal roadways. The above unfavorable factors led to the bolt easy to break off, and the surrounding rock and support structure had serious deformation and damage. It is shown that the roadway roof subsidence is large, the two sides shrink seriously, the floor bulges violently, the reinforcement mesh is exposed, and the concrete cracks.

2.1. Ground Stress Test.
In order to obtain the distribution law of the ground stress in the roadway of weak cementation stratum, YH3B-3 epoxy resin triaxial strain gauge was used in the 2# coal roadway of Hongqingliang mine to conduct the ground stress test according to the stress relief method, and 2 measuring points were arranged in total. The test results are listed in Table 1.

Table 1 shows that the 2# coal roadway in Hongqingliang mine is a tectonic stress field dominated by horizontal stress. The maximum horizontal principal stress is 1.45~1.56 times of the vertical stress. The ratio of the maximum horizontal stress to the minimum horizontal stress is 1.93~2.06. The two horizontal stresses differ greatly and have obvious directivity. The high horizontal stress is one of the main reasons for the deformation and destruction of the surrounding rock of the roadway, especially the internal extrusion of the two sides and the floor bulging.

2.2. Surrounding Rock Surface Displacement Monitoring.
In order to obtain the deformation characteristics of the surrounding rock of the weakly cemented roadway and the

TABLE 1: The roadway stress test results.

Number of measuring points	Principal stress (MPa)			Dip angle (°)			Azimuth angle (°)		
	σ_1	σ_2	σ_3	σ_1	σ_2	σ_3	σ_1	σ_2	σ_3
1#	12.37	16.33	4.52	69.22	14.16	15.62	87.61	23.11	169.24
2#	11.29	17.79	3.87	71.25	12.83	16.17	85.34	25.74	159.33
Average	11.83	17.06	4.20	70.24	13.49	15.89	86.48	24.43	164.29

control effect of the existing support scheme on the surrounding rock, the deformation of the surrounding rock was monitored.

The displacement of roadway surface shows a failure trend of larger failure rate in the early stage and smaller failure rate in the later stage. Although the deformation rate decreases in the later period, the deformation continues to increase (as shown in Figure 1). Within 0~15 d, the deformation rate of roadway is relatively high; the deformation rate slows down in 15~35 days. The maximum roof subsidence of the roadway is 640 mm, the floor heave is 400 mm, the left side deformation is 140 mm, and the right side deformation is 200 mm. The above monitoring data show that the roof is damaged to a large extent, followed by floor heave, and there is a certain degree of asymmetric deformation on both sides.

According to the data in Figure 1, it can be found that the surrounding rock deformation of the roadway is large, the deformation speed is fast, and the surrounding rock deformation and damage are serious. The above shows that the support mode of "bolt + anchor cable combined support" + "bolt mesh shotcrete" cannot effectively control the deformation of weak cementation roadway.

2.3. Stress Monitoring of Support Structure. In order to obtain the stress characteristics of the support structure, the dynamometer is used to monitor the stress of the anchor bolt and anchor cable. The relationship curve between the stress of the support structure and time is shown in Figure 2.

The initial pretightening force of the anchor cable is 140 kN, the pretightening force of the anchor bolt installed on the roof is 60 kN, and the pretightening force of the anchor bolt installed on the roadway side is 40 kN. The stress value of bolt and anchor cable in roadway decreases gradually with time. The rate of decline is large in the early stage and small in the late stage, as shown in Figure 2. In 0~15 d, the rate of force reduction is large. The rate of force reduction slows down within 15~35 days. The stress value of the anchor cable of the roadway is reduced to 75 kN, the stress value of the bolt installed on the roof is reduced to 21 kN, the stress value of the bolt installed on the left side is reduced to 20 kN, and the stress value of the bolt installed on the right side is reduced to 18 kN. After the excavation of the roadway, the roof settlement, floor heave, and deformation of both sides are large, resulting in an increase in the stress of the anchor bolt and anchor cable. The stress value of the anchor bolt and anchor cable increases continuously in the early stage. When the ultimate bearing capacity is reached, the support of the anchor bolt and anchor cable fails, and the stress value continues to decrease.

2.4. Deformation and Failure Characteristics of Roadway. The roof of the roadway sinks, the floor bulges, and the two sides extrude violently, and the failure pattern has certain asymmetry, and the failure of the side is mainly concentrated in the lower part. Some of the roadways are closed due to excessive deformation, and the surrounding rock deformation of the roadways does not stop after many times of renovation, resulting in the roadways cannot be used normally as shown in Figure 3.

3. Analysis of Influence of Chamber Group Project

After the stress of the surrounding rock is released after the excavation of the 3# coal chamber group, the vertical stress of the surrounding rock of 2# coal roadway is readjusted, which is mainly affected by the chamber group model composed of the auxiliary transport roadway, belt transport roadway, ventilation roadway, emergency roadway, water pump chamber, and power distribution chamber of 3# coal. As shown in Figure 4, when analyzing the influence of stress release after the excavation of the 3# coal chamber group on the stress distribution of the 2# coal roadway, take the 2# coal roadway opening as the origin, make the x-axis in the opposite direction of the excavation and the y-axis in the direction of the intersection roadway excavation to establish the coordinate system, and place the 3# coal chamber that affects the stress distribution of the 2 # coal roadway in the above coordinate system. In the model, the length of the affected section of the auxiliary transportation roadway is 230 m, and the affected length of the water pump chamber and the power distribution chamber is 55 m.

After calculation according to the theoretical model in Figure 5, the vertical stress distribution of 2# coal roadway is shown in Figure 6. It can be found that the vertical stress increment range of the roadway strata in 2# coal roadway is 2.1~4.0 MPa, which is 21%~40% higher than the initial stress due to the excavation of the cavern group in 3# coal chamber. When the rock stratum of 2# coal roadway is located directly above 3# coal chamber, its vertical stress appears a maximum, and there are five maximum points in the 149 m long failure zone of 2# coal roadway, respectively, corresponding to the auxiliary transportation roadway, belt transportation roadway, ventilation roadway, power distribution chamber, and emergency roadway of 3# coal chamber. Among them, the rock stratum of 2# coal roadway corresponding to ventilation roadway and emergency roadway is not completely at the maximum point of vertical stress, which is due to the influence of vertical stress superposition of 3# coal chamber.
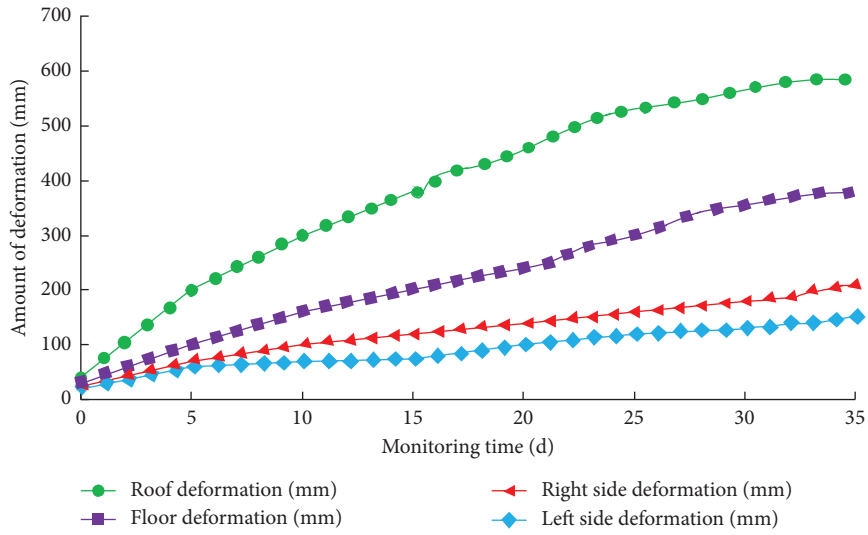
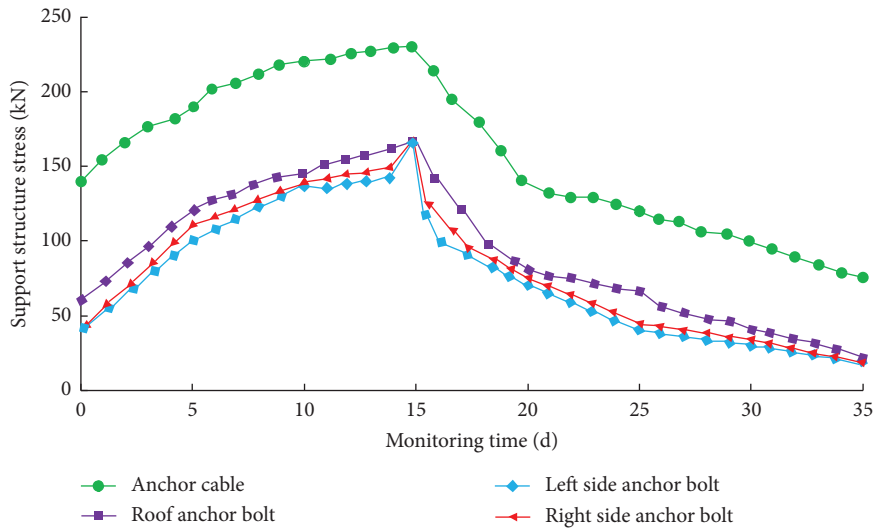Figure 1: Monitoring curve of roadway surface displacement.

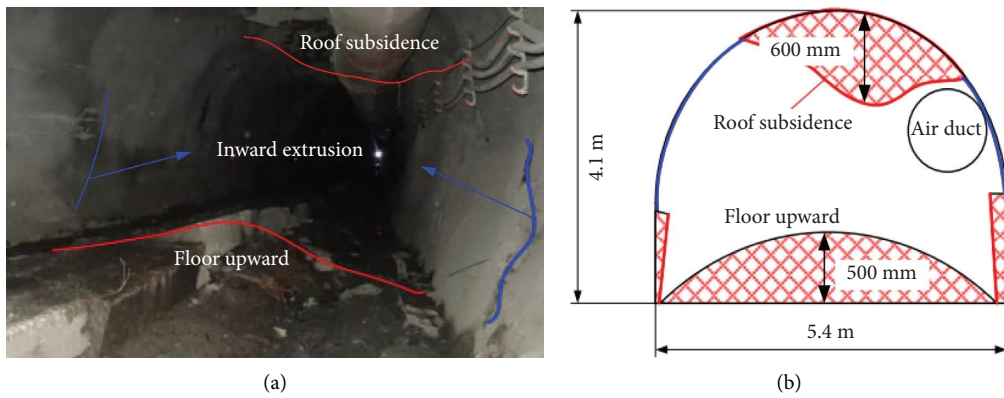Figure 2: Stress monitoring curve of support structure.

Figure 3: Schematic diagram of weak cemented roadway damage. (a) Roadway failure diagram and (b) sketch of roadway damage.
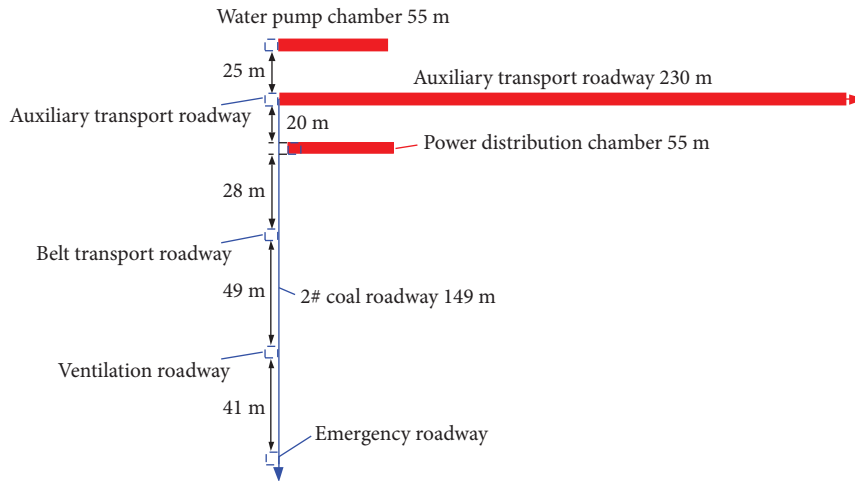
FIGURE 4: Schematic diagram of location relationship between 3# coal chamber and 2# coal roadway.
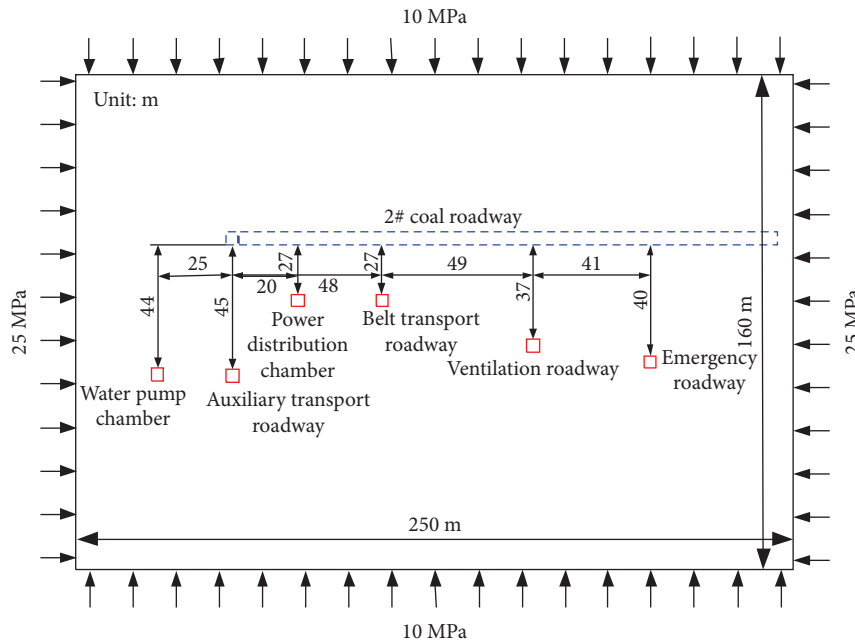

FIGURE 5: Stress release model of 3# coal chamber excavation.

The vertical distance between the 3# coal chamber group and the roadway rock stratum of 2# coal roadway is 27~45 m, which is equivalent to 7~11 times the chamber height. It shows that the vertical stress release after the excavation of the 3# coal chamber group acts on the rock stratum position of the 2# coal roadway, and the influence range of the vertical stress release can reach 7~11 times of the chamber height. In addition, the vertical stress increment of the belt transport roadway of 3# coal with a vertical distance of 27 m from the roadway of 2# coal is 4.0 MPa, and the vertical stress of the ventilation roadway with a vertical distance of 37 m from the roadway of 2# coal is 2.9 MPa, which indicates that the vertical distance and the size of the chamber are also the factors that affect the vertical stress distribution of the roadway of 2# coal when the cavern group of 3# coal is excavated.

4. Stability Control Technology of Surrounding Rock of Roadway

4.1. Mechanical Model and Parameter Calculation of Support. Combined with the stress condition of surrounding rock of coal roadway 2, considering the support effect of anchor bolt and anchor cable, the surrounding rock should be considered as the reinforcement arch structure when carrying out stress analysis, and the mechanical model of surrounding rock support structure is shown in Figure 7.

In the above mechanical model of surrounding rock support structure, a is the row spacing between bolts, m; b is the thickness of composite arch, m; q is the average load on the strengthened arch, kN/m^2; B is the width of roadway, m; Q is the anchoring force of anchor bolt, kN; σ_{t1} is the ultimate breaking force of a single
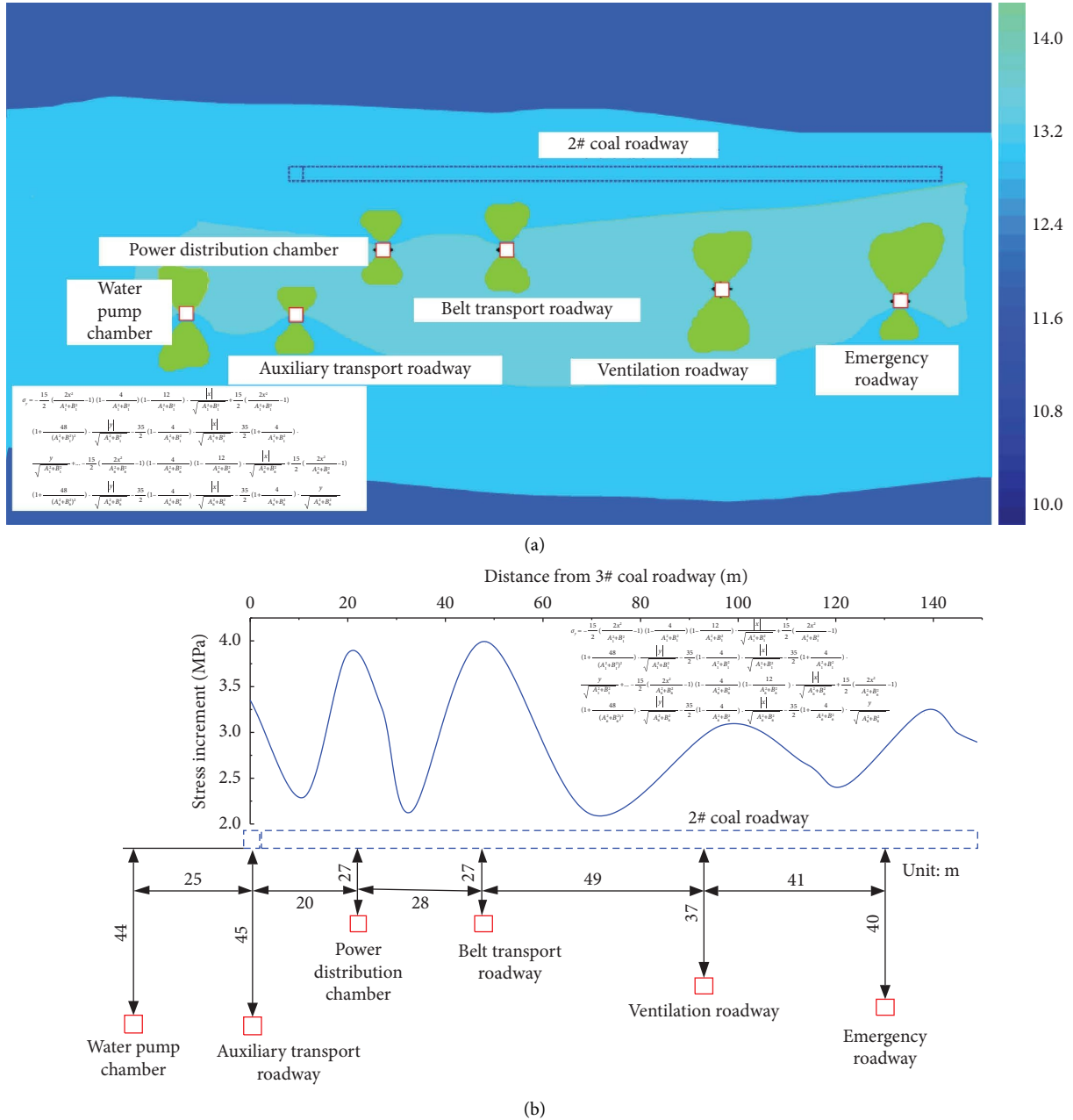
(a)

(b)

FIGURE 6: Calculation results of vertical stress adjustment of 2# coal roadway. (a) Vertical stress nephogram of 2# coal roadway and (b) vertical stress distribution curve of 2# coal roadway.

anchor cable, kN; L_{a1} is the anchoring length of the anchor cable, m; L_{a2} is the thickness of suspended unstable rock stratum, m.

According to the geological conditions of 2# coal roadway in Hongqingliang mine, the average unit weight of overburden γ is 2650 kN/m³; the thickness of unstable rock layer L_{a2} acting on the roadway roof is 5 m; the surplus coefficient k_1 is 1.2; the safety factor K is 1.8; the anchoring force Q of anchor bolt is 70 kN; the tensile strength σ_t is 3.8 MPa; the diameter d is 20 mm; the ultimate breaking force σ_{t1} of anchor cable is 355 kN; the net width B of roadway is 5 m.

4.1.1. Row Spacing between Bolts. The row spacing between bolts is calculated by using the reinforcement arch theory. The length of bolt L used in 2# coal roadway is 2.4 m. The row spacing between bolts is calculated by formula (1) [23]. Compared to the single bolt support theory or U-shaped steel shed support method, the study [23] combines the advantages of the above two methods, which can fully exert the bearing capacity of surrounding rock itself while improving the passive support capacity as much as possible.

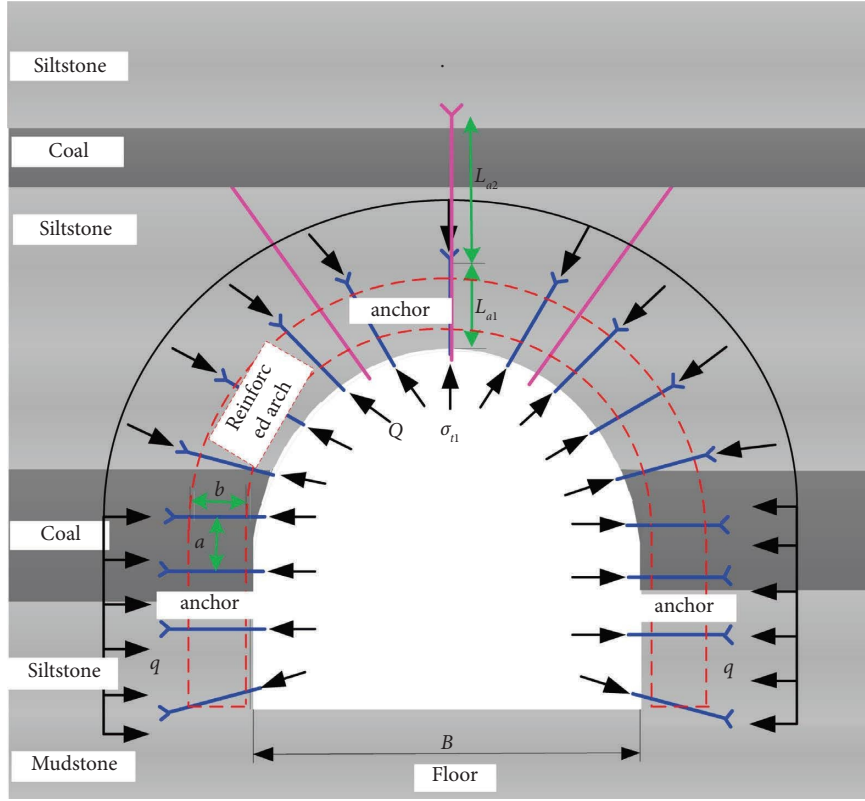$$L = L_1 + \frac{b \tan \alpha + a}{\tan \alpha}. \tag{1}$$

FIGURE 7: Mechanical model of surrounding rock support structure.

In formula (1), L is the anchor bolt length, m; L_1 is the exposed length of anchor bolt, m; b is the thickness of composite arch, m; α is the control angle in the rock mass where the bolt breaks, °; a is the row spacing between anchor bolts, m. According to the field measured data, L is 2.4 m, L_1 is 0.1 m, b is 1.5 m, and α is 45°, and the row spacing between bolts $a \leq 0.8$ m.

4.1.2. Anchor Rod Diameter. According to the strength principle of anchor bearing capacity and anchoring force, the anchor diameter can be determined by formula (2) [23].

$$d \geq k_1 \sqrt{\frac{4Q}{\pi \sigma_t}}. \tag{2}$$

In formula (2), d is the anchor rod diameter, mm; k_1 is the surplus coefficient; Q is the anchoring force of anchor rod, kN; σ_t is the tensile strength of anchor bolt, MPa. According to the field measured data, k_1 is 1.2, Q is 70 kN, and σ_t is 3.8 MPa. Substitute the above parameters into formula (2) to calculate $d \geq 18.4$ mm and determine the anchor rod diameter as 20 mm.

4.1.3. Length of Anchor Cable. The anchor cable has the function of suspending rock stratum, and the length of the anchor cable is calculated by formula (3) [23].

$$L_a \geq L_{a1} + L_{a2} + L_{a3} + L_{a4}. \tag{3}$$

In formula (3), L_a is the length of anchor cable, m; L_{a1} is the anchoring length of the anchor cable, m; L_{a2} is the thickness of suspended unstable rock stratum, m; L_{a3} is the thickness of supporting plate and anchorage, m; L_{a4} is the exposed length of anchor cable, m.

$$L_{a1} = \frac{\varphi_1 \times c}{\varphi_2^2 - \varphi_3^2}. \tag{4}$$

In formula (4) [23], φ_1 is the diameter of anchoring agent, mm; φ_2 is the drilling diameter, mm; φ_3 is the diameter of anchor cable, mm; c is the length of anchoring agent, m. According to the field measured data, L_{a1} is 1.6 m, L_{a2} is 5 m, L_{a3} is 0.15 m, and L_{a4} is 0.25 m. Considering the nonuniformity of the roof thickness, the safety factor is 1.4, and $L_a \geq 6.8$ m is calculated by formula (3), so the length of the anchor cable is 7300 mm.

4.1.4. Row Spacing between Anchor Cables. The anchor cable spacing is determined according to the rock weight borne by the anchor cable in case of anchor bolt failure and is determined by formula (5) [23].

$$S = \frac{3\sigma_{t1}}{4B^2 \gamma K}. \tag{5}$$

In formula (5), S is the row spacing between anchor cables, m; B is the roadway width, m; γ is the average unit weight of overlying strata, kN/m³; K is the safety factor; σ_{t1} is the ultimate breaking force of a single anchor cable, kN.
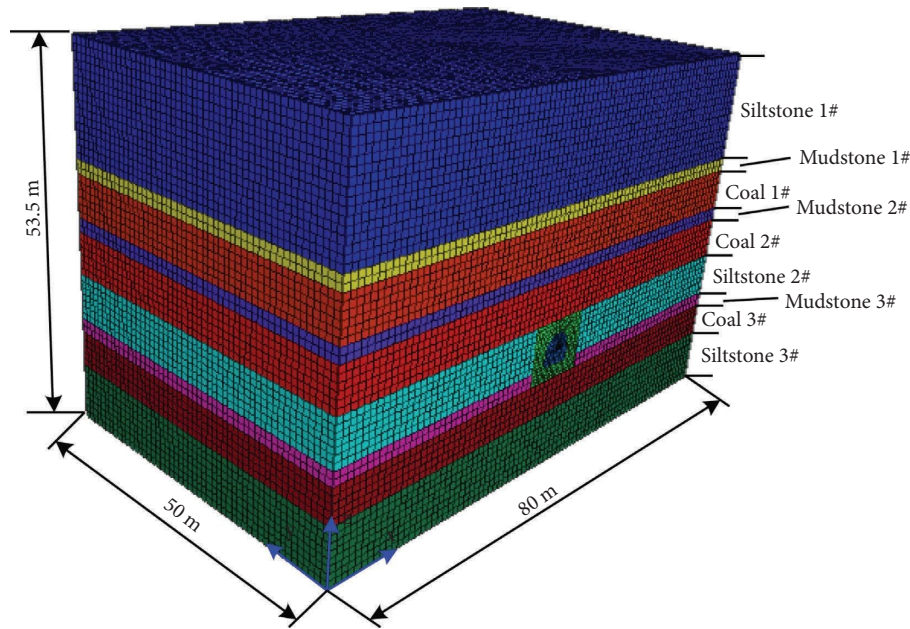
FIGURE 8: Numerical calculation model and meshing.

According to the field measured data, B is 5 m, γ is 2650 kN/m^3, K is 1.8, and σ_{t1} is 355 kN. S is 2.2 m is calculated by formula (5).

4.2. Support Simulation Research.

In order to fully compare the influence of support parameters on the surrounding rock control effect, the relationship between different support parameters and roadway displacement field, stress field is studied through numerical simulation to determine the reasonable support parameters of the roadway. The numerical calculation model is established by using FlAC3D, and the model size is $x \times y \times z = 80\,\text{m} \times 50\,\text{m} \times 53.5\,\text{m}$. In order to ensure the accuracy and efficiency of the calculation, the grids near the roadway are densified, the Mohr–Coulomb model is selected as the constitutive relationship of the model, and the surface contact Coulomb slip model is selected as the joint constitutive model. The top boundary of the model is a free boundary. The left and right and bottom boundaries of the model are displacement boundary conditions. The numerical calculation model and grid division are shown in Figure 8, and the physical and mechanical parameters of rock stratum are listed in Table 2.

Set U-shaped steel shed with spacing of 0.5 m (Scheme 1), 1 m (Scheme 2), and 1.5 m (Scheme 3), respectively, for simulation. The pretightening force of anchor bolt is 60 kN, and the pretightening force of anchor cable is 140 kN. The three simulation schemes study the repair and support effect of roadway surrounding rock from two aspects, including displacement field and stress field.

4.2.1. Analysis of Displacement Field.

According to Figures 9–11, in Scheme 1, the maximum roof subsidence of the roadway is 110 mm, the floor heave is 56 mm, the left side displacement is 82 mm, the right side displacement is 81 mm, and the distribution length of U-shaped steel shed axial force >170 kN is 2.03 m. In Scheme 2, the maximum roof subsidence of the roadway is 123 mm, the floor heave is 66 mm, the left side displacement is 85 mm, the right side displacement is 86 mm, and the distribution length of U-shaped steel shed axial force >170 kN is 2.74 m. In Scheme 3, the maximum roof subsidence of the roadway is 158 mm, the floor heave is 120 mm, the left side displacement is 98 mm, the right side displacement is 101 mm, and the distribution length of U-shaped steel shed axial force >170 kN is 4.19 m.

4.2.2. Analysis of Stress Field.

The vertical stress distribution of surrounding rock is basically consistent within the range of 0~4 m of the roadway, and the vertical stress of Scheme 1 is slightly less than that of Scheme 2. With the increase of the distance from the surrounding rock surface, Scheme 1 and Scheme 2 are more able to mobilize the bearing capacity of the deep stable rock mass than Scheme 3, and the vertical stress of the deep surrounding rock is correspondingly improved. Within the range of 0~1 m from the roadway surface, the vertical stress of roof surrounding rock in Scheme 1 is about 0.3 MPa and 2 MPa higher than that in Scheme 2 and Scheme 3, respectively, and the difference between the vertical stress of surrounding rock in Scheme 1 and Scheme 2 is very small (Figures 11–13).

From the surrounding rock deformation and stress distribution of the roadway, it is found that Scheme 1 and Scheme 2 can control the surrounding rock deformation more effectively than Scheme 3 after the comprehensive analysis. The difference between the repair and support effects of Scheme 1 and Scheme 2 is very small, but Scheme 2 can save a large economic cost compared with Scheme 1. Therefore, under the condition of ensuring the reliability of roadway repair and support, considering the economic cost factors, Scheme 2 is adopted for roadway repair and support.

TABLE 2: Rock layer physical and mechanical parameters table.

Name of rock stratum	Density (kg/m^3)	Bulk modulus (GPa)	Shear modulus (GPa)	Tensile strength (MPa)	Cohesion (MPa)	Internal friction angle (°)
Siltstone 1# Siltstone 2# Siltstone 3#	2450	0.70	0.49	0.96	4.84	40
Coal 1# Coal 2# Coal 3#	1300	0.41	0.23	0.20	0.34	29
Mudstone 1# Mudstone 2# Mudstone 3#	2620	0.39	0.24	0.25	2.42	40

(a)

(b)

(c)

FIGURE 9: Vertical displacement. (a) Scheme 1. (b) Scheme 2. (c) Scheme 3.
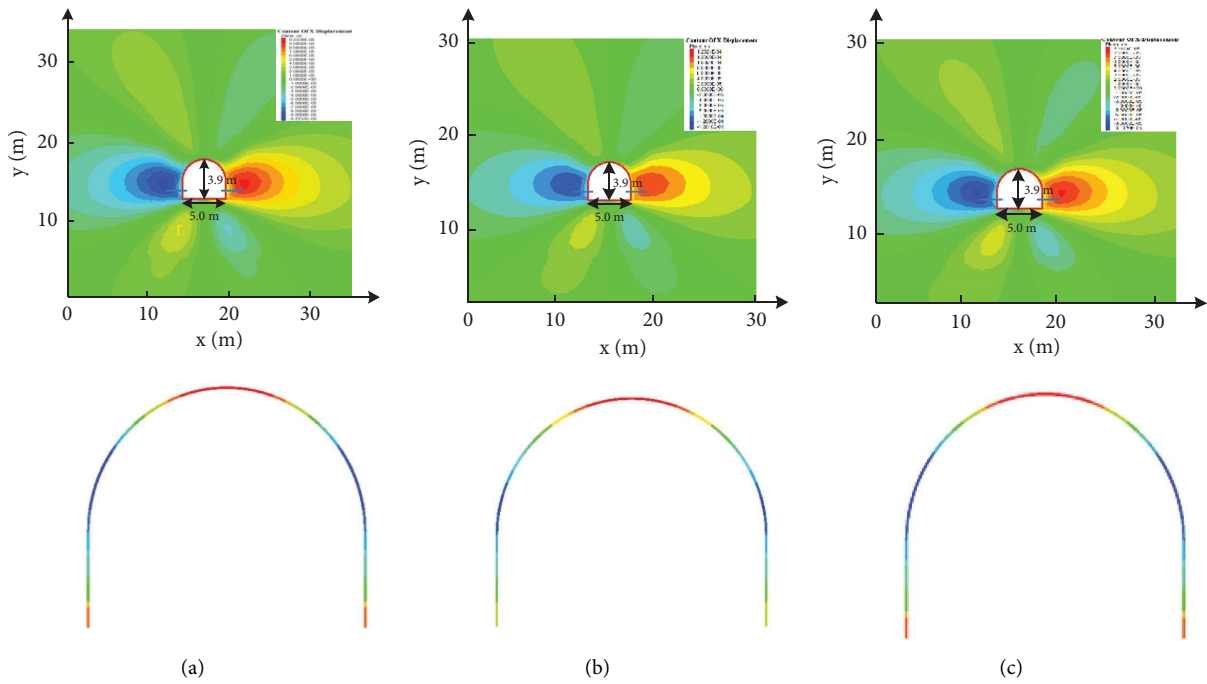

(a)

(b)

(c)

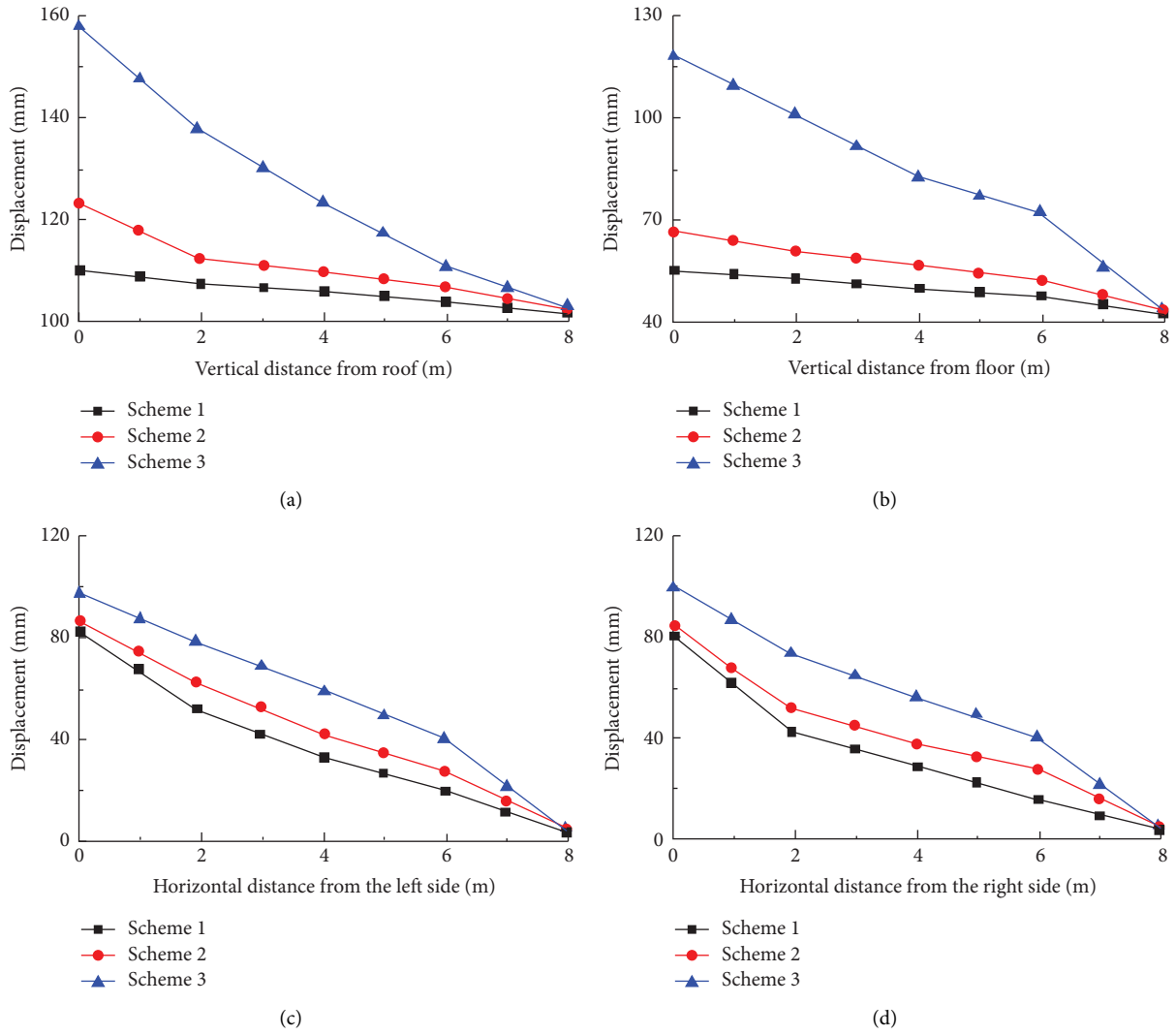FIGURE 10: Horizontal displacement. (a) Scheme 1. (b) Scheme 2. (c) Scheme 3.

Figure 11: Deformation at different positions of roadway. (a) Different positions of roof, (b) different positions of floor, (c) different positions of left side, and (d) different positions of right side.
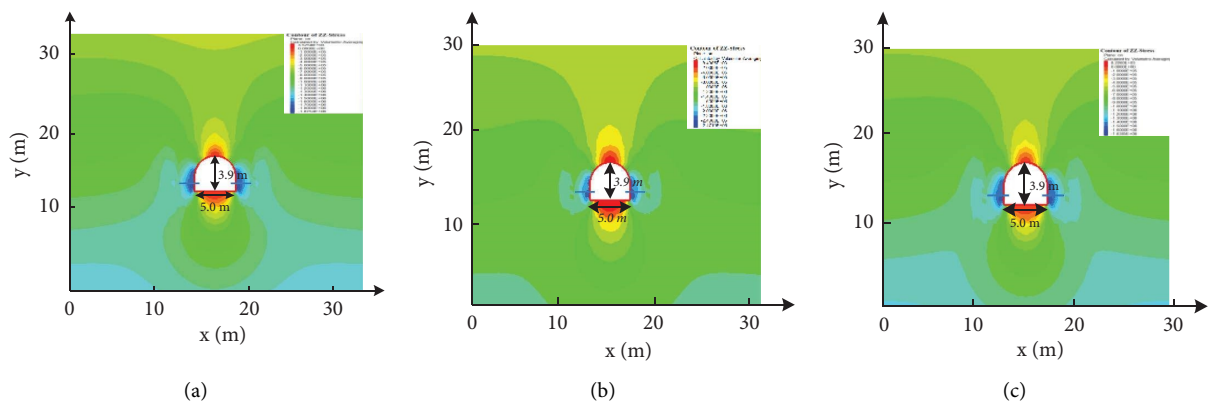

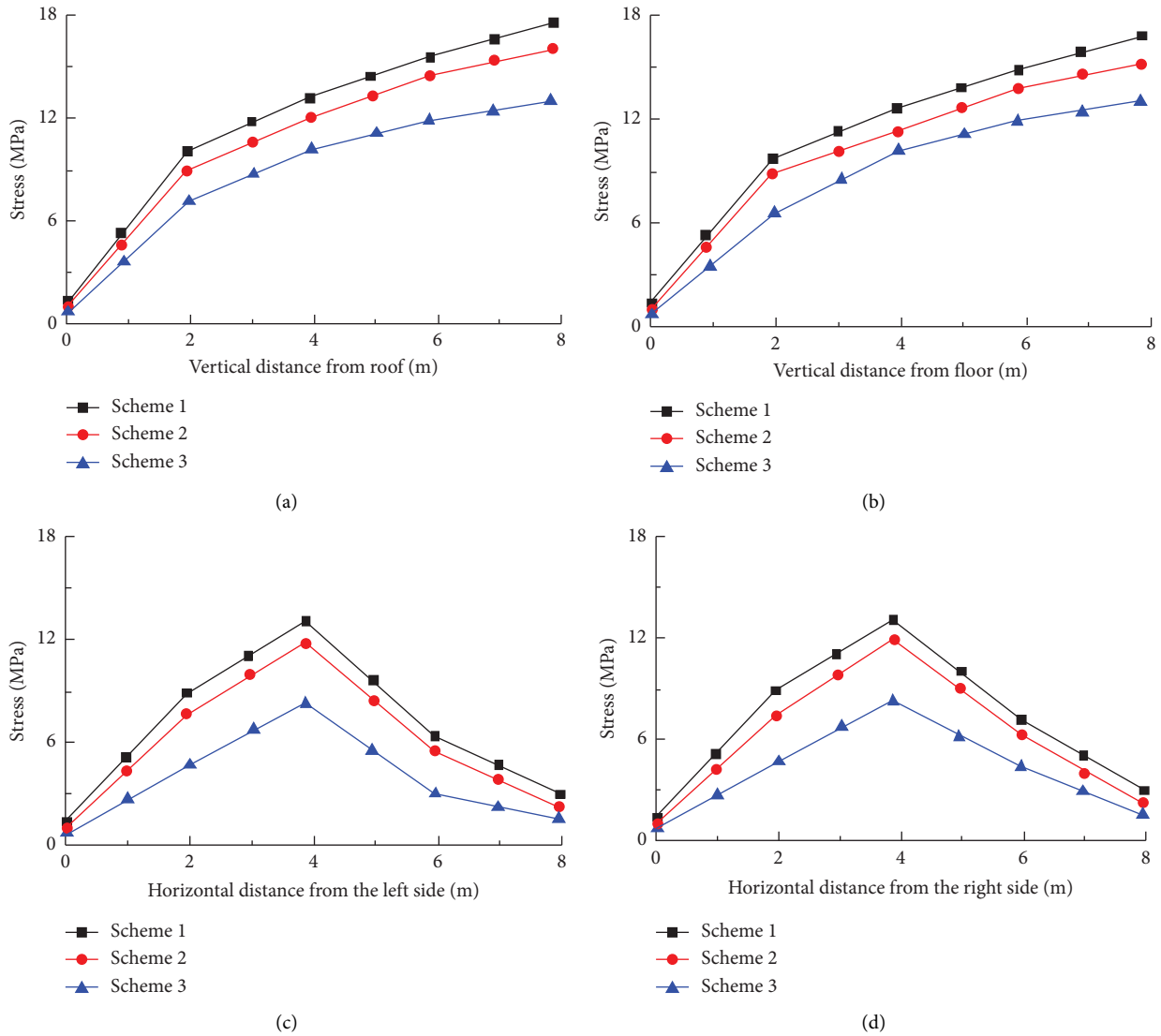Figure 12: Vertical stress. (a) Scheme 1. (b) Scheme 2. (c) Scheme 3.

FIGURE 13: Stress at different positions of roadway. (a) Different positions of roof, (b) different positions of floor, (c) different positions of left side, and (d) different positions of right side.

5. Conclusion

(1) After the excavation of the chamber group, the surrounding rock stress of the adjacent weakly cemented roadway would be adjusted. The vertical stress mainly expands in the vertical direction and the extension distance increases with the increase of the number of tunnels, which can affect the rock stratum position of 7–12 times the chamber's height. The horizontal stress mainly expands to the horizontal direction, and the extension distance increases with the increase of the number of tunnels, which can affect the rock stratum position of 3–6 times the chamber's width. The stress concentration of weakly cemented rock stratum is mainly affected by the vertical stress released by the chamber group.

(2) According to the support concept of "allowable deformation + stress release + controlled form," the roadway support technology of U-shaped steel + shed leg bolt + steel mesh floor "control form," flexible material wall filling with "allowable deformation + stress release" is established. After the U-shaped steel support is filled behind the wall and strengthened at key parts, the support strength surrounding rock deformation curve shows a change law of slow increase in the initial stage, approximate linear increase in the middle stage, and slow decrease in the later stage.

(3) The surface displacement of the cemented soft rock roadway has not changed, which ensures that the deformation and failure of the surrounding rock of the roadway are within a reasonable range, and realizes the safety and normal use of the roadway.

Data Availability

All data, models, and code generated or used during the study appear in the submitted article.

Conflicts of Interest

The author declares that there are no conflicts of interest with any individual/organization for the present work.

Acknowledgments

References

[1] W. Zhang, T. B. Zhao, and M. L. Xing, "Research on instability mechanism and supporting countermeasures of weakly cemented roadway in adjacent chamber group engineering," *Preprint*, 2022.

[2] T. B. Zhao, W. Y. Guo, and Y. L. Tan, "Case studies of rock bursts under complicated geological conditions during multi-seam mining at a depth of 800 m," *Rock Mechanics and Rock Engineering*, vol. 51, no. 5, pp. 1539–1564, 2018.

[3] T. B. Zhao, W. Zhang, S. T. Gu, Y. W. Lv, and Z. H. Li, "Study on fracture mechanics of granite based on digital speckle correlation method," *International Journal of Solids and Structures*, vol. 193-194, pp. 192–199, 2020.

[4] W. Zhang, W. Y. Guo, and Z. Q. Wang, "Influence of lateral pressure on mechanical behavior of different rock types under biaxial compression," *J. Cent. South Univ.*, vol. 29, no. 11, pp. 3695–3705, 2022.

[5] W. Zhang, B. L. Zhang, and T. B. Zhao, "Study on the law of failure acoustic–thermal signal of weakly cemented fractured rock with different dip angles," *Rock Mechanics and Rock Engineering*, 2023.

[6] M. C. He, "Progress and challenges of soft rock engineeringin depth," *Journal of China Coal Society*, vol. 39, no. 8, pp. 1409–1417, 2014.

[7] K. Zhou, F. H. Yu, Y. L. Tan, H. Cheng, and W. Guo, "In-situ investigation on fractured evolution law of surrounding rock in weakly cemented soft rock roadway," *Energy Sources Part A*, 2021.

[8] J. Shang, S. R. Hencher, and L. J. West, "Tensile strength of geological discontinuities including incipient bedding, rock joints and mineral veins," *Rock Mechanics and Rock Engineering*, vol. 49, no. 11, pp. 4213–4225, 2016.

[9] G. B. Chen, Y. Li, T. Li, and G. Zhang, "Deterioration law of intermittent jointed sandstone mechanical properties under water-rock interaction," *Acta Geophysica*, vol. 70, no. 4, pp. 1923–1935, 2022.

[10] A. Harrypersad-Daniel, O. O. Blake, and R. Ramsook, "Determining the static Young's modulus and Poisson's ratio, and compressive strength of the friable Erin Formation rocks using P-wave velocity," *Journal of Applied Geophysics*, vol. 198, Article ID 104557, 2022.

[11] Q. B. Meng, L. J. Han, W. G. Qiao, D. Lin, and J. Fan, "Support technology for mine roadways in extreme weakly cemented strata and its application," *International Journal of Mining Science and Technology*, vol. 24, no. 2, pp. 157–164, 2014.

[12] P. Zhang, D. Gearhart, M. V. Dyke, D. Su, E. Esterhuizen, and B. Tulu, "Ground response to high horizontal stresses during longwall retreat and its implications for longwall headgate support," *International Journal of Mining Science and Technology*, vol. 29, no. 1, pp. 27–33, 2019.

[13] M. Chen, W. B. Lu, W. J. Zhang, P. Yan, and C. Zhou, "An analysis of consolidation grouting effect of bedrock based on its acoustic velocity increase," *Rock Mechanics and Rock Engineering*, vol. 48, no. 3, pp. 1259–1274, 2015.

[14] H. P. Kang, H. W. Lv, F. Q. Gao, X. Meng, and Y. Feng, "Understanding mechanisms of destressing mining-induced stresses using hydraulic fracturing," *International Journal of Coal Geology*, vol. 196, pp. 19–28, 2018.

[15] Q. Wang, H. K. Gao, H. C. Yu, B. Jiang, and B. Liu, "Method for measuring rock mass characteristics and evaluating the grouting-reinforced effect based on digital drilling," *Rock Mechanics and Rock Engineering*, vol. 52, no. 3, pp. 841–851, 2019.

[16] Y. T. Sun, G. C. Li, J. F. Zhang, and D. Qian, "Stability control for the rheological roadway by a novel high-efficiency jet grouting technique in deep underground coal mines," *Sustainability*, vol. 11, no. 22, p. 6494, 2019.

[17] X. J. Yang, E. Y. Wang, Y. J. Wang, Y. Gao, and P. Wang, "A study of the large deformation mechanism and control techniques for deep soft rock roadways," *Sustainability*, vol. 10, no. 4, p. 1100, 2018.

[18] Y. L. He, M. S. Gao, D. Xu, and X. Yu, "Investigation of the evolution and control of fractures in surrounding rock under different pressure relief and support measures in mine roadways prone to rockburst events," *Royal Society Open Science*, vol. 8, no. 3, Article ID rsos.202044, 2021.

[19] J. W. Zheng, W. J. Ju, and X. D. Sun, "Differentiation response characteristic of roadway deformation and rock supporting analysis," *J. Min. Strata Control Eng.*, vol. 3, no. 3, 2021.

[20] X. W. Zhang, J. H. Xu, and Z. B. Liu, "Mechanical response and deformation of weak interbedded mudstone under different loading paths," *J. Min. Strata Control Eng.*, vol. 3, no. 4, 2021.

[21] Z. Y. Fan, Y. L. Li, and H. Sun, "Characteristics and control measures of unsymmetric deformation of roadways within weakly-cemented soft rock," *J. Min. Strata Control Eng.*, vol. 4, no. 2, 2022.

[22] Z. Y. Wang, P. F. Jiang, and X. Z. Meng, "Numerical study of support effectiveness and mechanism of pre-stressed bolts," *J. Min. Strata Control Eng.*, vol. 4, no. 4, 2022.

[23] Y. Feng, J. P. Harrison, and N. Bozorgzadeh, "Uncertainty in in situ stress estimations: a statistical simulation to study the effect of numbers of stress measurements," *Rock Mechanics and Rock Engineering*, vol. 52, no. 12, pp. 5071–5084, 2019.